Available online at www.sciencedirect.com

ScienceDirect

Energy Procedia 00 (2013) 000–000

Energy Procedia

www.elsevier.com/locate/procedia

GHGT-12

Numerical simulation of CO_2 dispersion from punctures and ruptures of buried high-pressure dense phase CO_2 pipelines with experimental validation

Christopher J. Wareing[a,b*], Michael Fairweather[a], Robert M. Woolley[a], Samuel A.E.G. Falle[b]

[a]*School of Chemical and Process Engineering, University of Leeds, Leeds, LS2 9JT, United Kingdom*
[b]*School of Mathematics, University of Leeds, Leeds, LS2 9JT, United Kingdom*

Abstract

Carbon capture and storage (CCS) presents an option for significantly reducing the amount of carbon dioxide (CO_2) released into the atmosphere and mitigating the effects of climate change. Pipelines are considered to be the most likely method for transporting captured CO_2 and their safe operation is of paramount importance as their contents are likely to be in the region of several thousand tonnes and CO_2 poses a number of concerns upon release due to its unusual physical properties. To this end, National Grid initiated the COOLTRANS (CO_2 Liquid Pipeline Transportation) research programme to consider the pipeline transportation of high-pressure dense phase CO_2. Part of this work involved the development of a mathematical model for predicting the dispersion of pure CO_2 following the venting, puncture, or rupture, of such a transportation pipeline during normal operational conditions. In this paper, we describe the use of a computational fluid dynamic (CFD) tool that can be used to numerically simulate the near-field sonic dispersion from such releases, above and below ground. The model is shown to qualitatively and quantitatively reproduce observed experimental results. Validated flows at the top of the crater formed by below ground releases presented here for a range of scenarios provide the basis for developing robust source conditions for use in CFD studies of far-field dispersion, and for use with pragmatic quantified risk assessment (QRA) models.

Selection and peer-review under responsibility of GHGT.

Keywords: CCS transport, multi-phase flow, experimental measurement, mathematical modelling, accidental releases, atmospheric dispersion

The Don Valley CCS Project is co-financed by the European Union's European Energy Programme for Recovery
The sole responsibility of this publication lies with the author.
The European Union is not responsible for any use that may be made of the information contained therein.

* Corresponding author. Tel.: +44-113-343-3871; fax: +44-113-343-5090.
E-mail address: C.J.Wareing@leeds.ac.uk

Selection and peer-review under responsibility of GHGT.

1. Introduction

Carbon capture and storage (CCS) refers to a set of technologies designed to reduce carbon dioxide (CO_2) emissions from large point sources of emission, such as coal-fired power stations, in order to mitigate greenhouse gas release. CCS technology, or sequestration, involves capturing CO_2 and then storing it in a suitable storage facility, instead of allowing its release into the atmosphere where it contributes to climate change. Necessary transportation can be achieved in different ways, but it is commonly acknowledged that high pressure pipelines transporting liquid CO_2 will be the most reliable and cost effective choice. For the design and risk assessment of such pipelines, a quantitative understanding of the consequences of an accidental or operational high-pressure release is required. The fluid dynamic modelling of CO_2 poses a unique set of problems due to its unusual phase transition behaviour and physical properties. Liquid CO_2 has a density comparable with that of water, but has a viscosity of magnitude more frequently associated with gases. These properties make the transport of dense phase CO_2 an economically viable and attractive proposition. However, due to it possessing a relatively high Joule-Thomson expansion coefficient, calculations and experimental evidence indicate that the rapid expansion of an accidental release may reach temperatures below -100 °C in some circumstances. Due to this effect, solid CO_2 formation following a pipeline puncture or rupture is to be expected, whether directly from liquid or via a vapour-phase transition. Additionally, CO_2 sublimes at ambient atmospheric conditions, which is a behaviour not seen in most other solids, and is an additional consideration when modelling flows such as these. Predicting the correct fluid phase during the discharge process in the near-field is of particular importance given the very different hazard profiles of CO_2 in the gas and solid states. The safe operation of CO_2 pipelines is of paramount importance then, as the inventory associated with a cross-country pipeline would likely be several thousand tonnes, and CO_2 is a colourless, odourless asphyxiant which sinks in air. It is directly toxic in inhaled air at concentrations above about 5% and is likely to be fatal in a short time period at concentrations around 10% under certain conditions. This paper describes the application of a mathematical model to various accidental or operational scenarios, including validation against relevant experimental data, specifically 1) vertical dense phase and gas phase sonic releases of high-pressure CO_2 through 25.4mm (1-inch) nominal diameter venting pipes, 2) punctures of buried high pressure pipelines carrying dense phase CO_2 and 3) ruptures of the same buried pipelines. The predictions are based on solutions of the transport equations for mass, momentum and total energy, with closure achieved using a compressibility-corrected k-ε turbulence model. A non-ideal equation of state with additional formulations to predict solid phase properties is also implemented to describe the thermodynamic characteristics of CO_2.

2. Mathematical modelling

2.1. Turbulent flow field

The calculations employed an adaptive finite-volume grid algorithm which uses a two- or three-dimensional rectangular mesh with grid adaption achieved by the successive overlaying of refined layers of a computational mesh [1]. Where there are steep gradients of variable magnitudes, such as at flow boundaries or discontinuities such as a Mach shock, the mesh is more refined than in areas such as the free stream of the surrounding fluid. This technique enables the generation of fine grids in regions of high spatial and temporal variation and, conversely, coarser grids where the flow field is numerically smooth. The model to describe the fluid flow field employed for dense phase and gas phase CO_2 vertical releases was cast in an axisymmetric geometry. The model for the buried puncture and rupture releases was cast in three-dimensional Cartesian coordinates, with an axis of symmetry along the axis of the release. The standard transport equations for modelling fluid flow representing continuity, momentum, turbulence kinetic energy and its dissipation rate, mixture fraction, and the total energy per unit volume (internal energy plus kinetic energy) were solved. They were implemented with the inclusion of a two-equation turbulence model [2] used to represent the turbulent Reynolds stresses. Although this standard k-ε model has been extensively used for the prediction of incompressible flows, its performance is well known to be poor in the prediction of their compressible counterparts; the model consistently over-predicts turbulence levels, and hence mixing, due to compressible flows displaying an enhancement of turbulence dissipation. A number of modifications to the k-ε model have been proposed by various authors, and previous work [3] has indicated that for flows typical

of those being studied here, the model proposed by Sarkar et. al. [4] provides the most reliable predictions. This model specifies the total dissipation as a function of a turbulent Mach number, and was derived from the analysis of direct numerical simulations of the exact equations for the transport of the Reynolds stresses in compressible flows. Solutions of the equation set were obtained for the time-dependent, density-weighted forms of the descriptive equations, and the integration was performed by a shock-capturing conservative, upwind second-order accurate Godunov numerical scheme [5]. A Harten, Lax and van Leer Riemann solver [6] was employed to calculate fluxes at cell boundaries.

2.2. Non-ideal equation of state

The phase equilibrium and transport properties for CO_2 were partly determined using the Peng-Robinson equation of state for CO_2 [7]. This is satisfactory for the gas phase, but not for the condensed phase. In addition, it is not accurate for the vapour pressure below the triple point, as it does not consider physical phenomena such as the latent heat of fusion. Hence, a composite equation of state was constructed whereby the vapour phase was calculated using the Peng-Robinson equation, and the condensed phases and the vapour pressure calculated using tabulated values from Span and Wagner [8] and the DIPPR® Project 801 Database[†]. Calculations were undertaken using the Helmholtz free energy in terms of temperature and molar volume as all other thermodynamic properties can be readily obtained from it. A full description of this non-ideal equation of state with additional formulations to accurately predict solid phase properties including the latent heat of fusion is described elsewhere [9].

2.3. Homogeneous equilibrium and relaxation models

In a homogeneous equilibrium model, all phases are assumed to be in dynamic and thermodynamic equilibrium. That is, they all move at the same velocity and have the same temperature. In addition, the pressure of the CO_2 vapour is assumed to be equal to the saturation pressure whenever the condensed phase is present. The pressure of the condensed phase CO_2 is also assumed to be equal to the combined pressure of CO_2 vapour and air (the total pressure). These assumptions are reasonable provided any CO_2 liquid drops or solid particles are sufficiently small. The computational implementation assumed that the mixture was in homogeneous equilibrium, i.e. that the solid/liquid and gas phases were well mixed and that the liquid drops or solid particles were sufficiently small. However, there are some indications from recent experimental work that this is not true [10] for small-diameter releases. For the current model, a simple sub-model for the relaxation to equilibrium was therefore included when necessary. A full model will require the complete inclusion of drops and/or particles and is in development.

3. Experimental arrangement

Experiments were carried out by DNV GL [11], working on behalf of National Grid, as part of the COOLTRANS research programme [12] in order to study the deliberate discharge of dense phase CO_2 in various scenarios. In the venting scenarios, a vertical vent pipe configuration was arranged so that an approximately steady flow was produced through the vent pipe for a minimum period of 30 seconds. The experiments were performed at the DNV GL Spadeadam test facility in Cumbria, UK. The rig consisted of the following four main components: a buffer pipe, a main CO_2 storage vessel, a supply pipe and a vent pipe. The buffer pipe was a 150 mm diameter pipe of 132 m length that sloped downwards from its connection with a high pressure nitrogen reservoir at the upper end to the CO_2 storage vessel at the other end. The CO_2 storage vessel was a 600 mm diameter horizontal vessel of 24 m in length. It was able to be filled independently from a large refrigerated CO_2 storage vessel or from the buffer pipe. The supply pipe was a horizontal pipe of 50 mm diameter and 12 m length that was connected to the main storage vessel at one end by a flexible pipe and, having turned through 90^o at an elbow, to the vertical vent pipe at its other end. The vent pipe was a length of pipe that was connected to the supply pipe at one end and was open to the atmosphere

[†] Knovel Library, Imperial College London, 2011. Available from: http://www3.imperial.ac.uk/library/find/databases/knovellibrary

at the other. Vent pipes of 25 mm diameter and 3 m long were used in the cases considered here. Measurements of the dispersing jet temperature were made on two horizontal planes at 4 m and 7 m above the vent exit.

The rig used to study the behaviour of punctures in a buried pipeline consisted of a remote, high pressure nitrogen reservoir, connected to a long length of gently sloping charge line of outside diameter 304.8 mm which was filled with dense phase CO_2 at a slightly lower pressure. The charge line was connected to the test section, consisting of a horizontal section of pipeline of outside diameter 914 mm and of length approximately 16.5 m. The test section was buried so that the pipe crown was at a depth of 1.2 m below the local ground level. The pipeline was fitted with a number of outlet ports around its perimeter in order to carry out a series of simulated puncture experiments from a buried dense phase CO_2 pipeline. In each experiment, all of the outlets except one were fitted with blanking plates to prevent release. However, one outlet was fitted with a bursting disk that was designed to fail once a set pressure level was exceeded. In the cases that have been simulated here, 'pre-formed' craters were constructed around the release location to simulate the shape of the crater formed in earlier experiments. These were not re-filled with soil and so the release in this experiment was into air. The lack of soil backfill meant that instrumentation could be deployed immediately above the crater on two horizontal planes at 1 m and 2 m above ground level, with thermocouples attached to a suspended frame. It is to these experimental data that pucture comparisons are made in the next section.

In the case of investigating rupture behaviour, a ¼-scaled experiment was performed. A 230 m long length of 152 mm external diameter pipeline was buried horizontally at a depth of 300 mm and connected at each end through remotely-operated valves to separate 914 mm outside diameter 'reservoir' pipes. An approximately 3 m long test section was removed from the middle of the 152 mm diameter pipeline. The open ends created by the removal of this test section were held in place by buried anchor blocks. The 152 mm pipeline was instrumented with pressure transducers and thermocouples and measurements were made at ground level of the concentration and temperature within the dispersing CO_2 cloud that was produced. The particular release considered here took place into a preformed crater below ground, based on previous experiments. There was no soil backfill in the crater and so the release took place into air. Since this experiment took place into a preformed crater with no backfill, it was possible to place an array of temperature thermocouples 1 m above the crater. It is to these experimental data that rupture comparisons are made in the next section.

4. Results and discussion

4.1. Vertical vent free releases

Figure 1 shows the experimental data from, and predictions of, the dense phase CO_2 vertical vent release. In the left panel, the data and predictions at 4 m above the vent are shown, with the right panel giving the data and predictions at 7 m above the vent. The predicted core temperature of the jet is in very good agreement with the data in both cases. The predicted width of the jet is also in good agreement with those data. Some spread of the data can be understood in terms of the atmospheric conditions at the time as a 2.5 ms^{-1} wind was blowing from the west-south-west which compressed the jet towards the axis on the sides of the jet exposed to this atmospheric flow, as discovered when viewing the data by compass quadrant. Figure 2 shows the experimental data from, and predictions of, the gas phase CO_2 vertical release. In the left panel the data and predictions at 4 m above the vent are shown, with the right panel again giving equivalent results at 7 m above the vent. Despite the considerably different temperature range observed as compared to the dense phase CO_2 release, the predicted core jet temperatures and widths are again in good agreement with the data on both planes. More information regarding the quantitative and qualitative validation of the model for free releases can be found elsewhere [13, 14].

4.2. Punctures of buried pipelines

Figure 3 shows visualisations of the simulations of puncture scenarios. In Figure 3 (a), (b) and (c) a side puncture release horizontally from a buried pipeline into a pre-formed crater is presented. The Mach shock structure can clearly be seen ~0.2 m from the release point in panel (c). Atmospheric pressure is reached immediately post Mach shock. When the jet impacts on the opposite crater wall, the flow is divided downwards into the crater and upwards

along the crater wall. The bottom half of the crater is eventually filled with cooled CO_2, 30% dense phase, at the sublimation temperature of 194.25 K. The upward jet emerges from the crater at a velocity of approximately 25 ms^{-1} following the angle of the crater wall. The jet contains approximately 50% CO_2, 25% of that in the solid phase at the crater rim. The prediction 1 m above the crater is compared to experimental data in panel (1). The experimental data are presented time averaged from t=25 to t=50 seconds during the release. The experimentally observed data points do not show the same temperature range as the prediction, but do show the same trend, indicating agreement in the size of the cloud leaving the crater. The simulation is able to predict the correct quantitative temperature range in the cloud coming out of the crater. The low temperatures in the cloud indicate that solid phase CO_2 is likely to be present. The simulation is also able to predict the correct qualitative size of the release coming out of the crater.

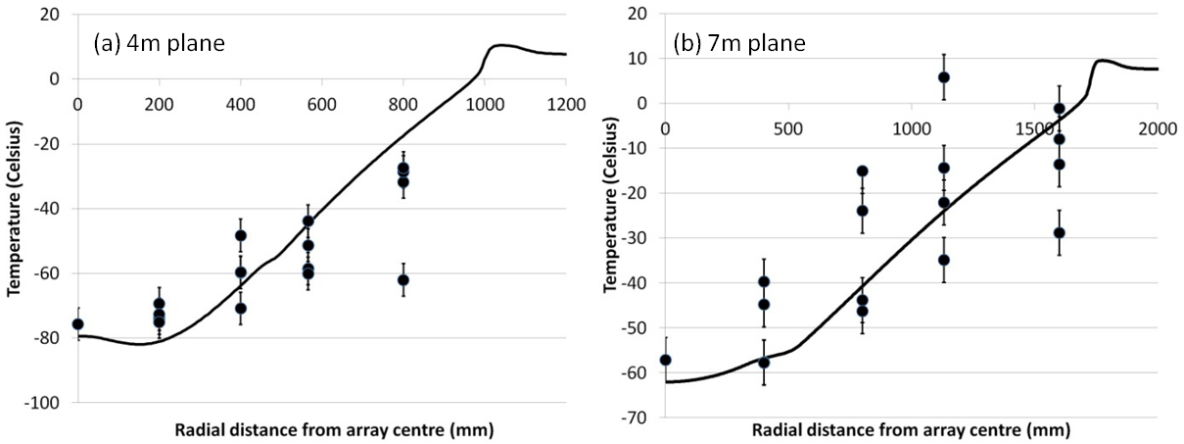

Figure 1. Dense phase CO_2 vertical release. Data (markers) and model predictions (solid line) are shown on the planes 4 m (a) and 7 m (b) above the vent. For more information, see [12].

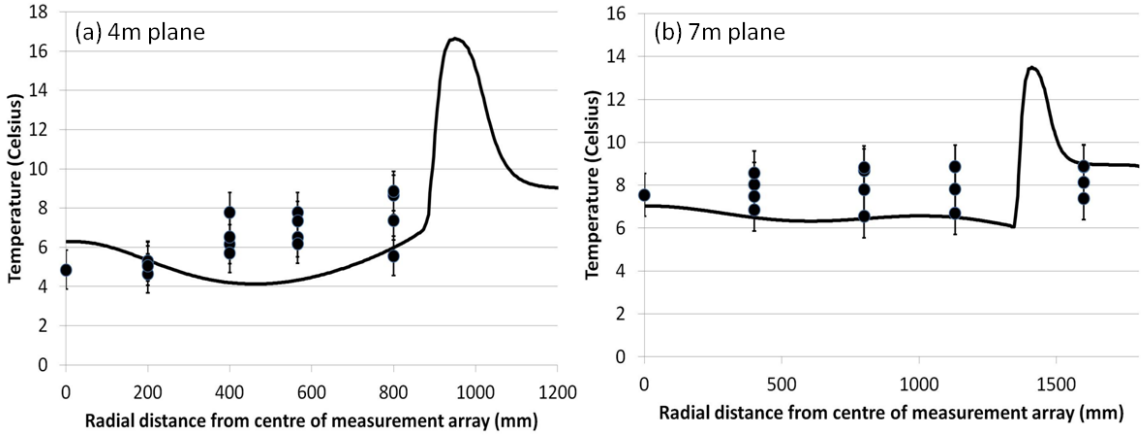

Figure 2. Gas phase CO_2 vertical release. Data (markers) and model predictions (solid line) are shown on the arrays 4m (a) and 7m (b) above the vent. For more information, see [12].

A slice through the simulation of the bottom puncture scenario is shown in Figure 3(d). Specifically, simulated flow temperature is shown on a vertical slice perpendicular to the pipeline, at the position of the puncture. The entire domain has been filled by a cloud of cold CO_2. The downwards jet at the base of the pipeline is indicated by the position of the Mach shock, a short distance below the pipeline. The coldest temperatures and lowest densities are reached just before the Mach shock. The CO_2 fraction at this time is still 100%. As previously, post-Mach shock a jet forms pointing downwards, this time towards the base of the crater and consisting of a cold slow moving ‘core’ surrounded by a fast moving ‘sheath’. This structure exists only for a very short distance as the jet impacts onto the

base of the crater. It is deflected away from the middle of the base of the crater and towards the sides, where it then moves up the crater wall. Given that the entire momentum of the jet is downwards from the puncture and the base of the crater is only slightly curved, the high speed jet is transformed into a slow speed plume filling up the crater and eventually spreading over the sides of the crater. There is an upwards plume in this prediction, the maximum height reached of which is in reasonably good agreement with experimental observations.

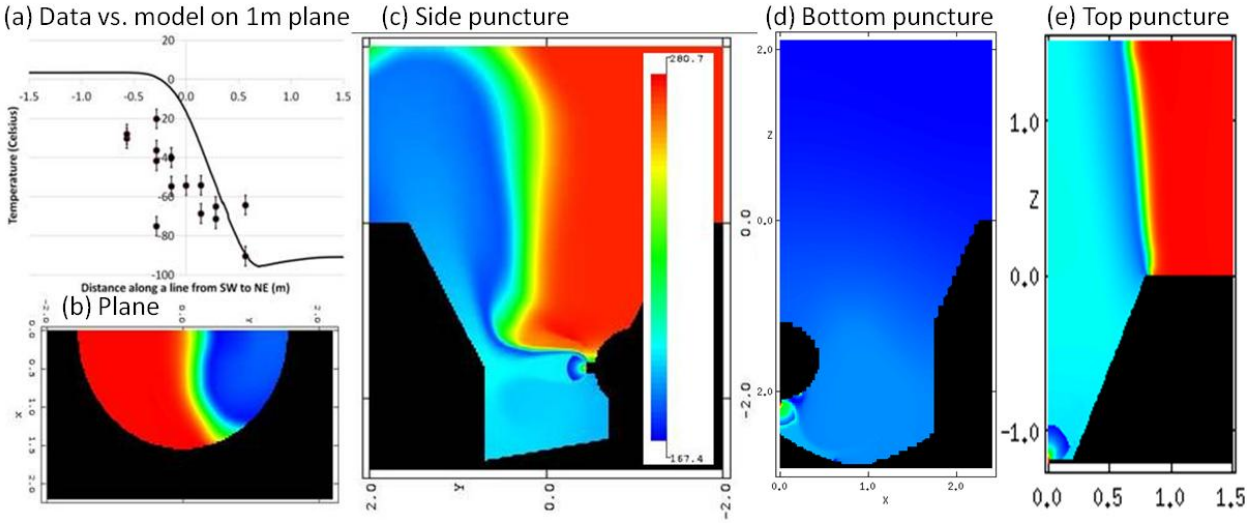

Figure 3. A simulated puncture release from a high-pressure dense phase CO_2 buried pipeline. (a) a comparison of model predictions (line) with data (markers) on the 1m plane above the crater (z=1) in a side puncture case; (b) predicted temperatures at the crater rim (z=0) in a side puncture case; (c) a slice through the centre of the crater on the symmetry plane (x=0) showing the predicted temperatures in a side puncture case; (d) a slice through the centre of the crater perpendicular to the symmetry plane (x=0) showing the predicted temperatures in a bottom puncture case; and (e) a plot of the temperature in an axisymmetric simulation of a top puncture case.

In Figure 3(e) we present the simulated axisymmetric flow in the case of a top puncture in a pipeline. The expansion zone terminated by the Mach shock is clear at the puncture. Beyond the Mach shock, the flow expands to fill the crater and is hence pure CO_2 until almost the crater rim. The temperature in the flow is at the sublimation temperature. The crater appears to act as a large expansion nozzle into which the flow expands and slows down to fill it post-Mach shock. Hence the flow contains 100% CO_2 until just below the top of the crater, with approximately 35% solid fraction in the core. It is only at the rim of the crater where air is able to mix into the flow. The velocity of the flow at the crater edge is on the order of 28 ms^{-1} in the core, creating a large plume directly above the crater in agreement with photographic evidence from the experimental tests. This is of a magnitude not dissimilar to that numerically predicted for the side puncture. The experimental plume behaviour between the two tests is not that different either, lending support to this prediction. There is a slight pressure expansion at the crater rim, as the pressure is approximately 8% above atmospheric pressure, but this is not large and probably a consequence of the expansion nozzle nature of the crater. More information on the behaviour of puncture releases will be available elsewhere in due course [15]; Table 1 reproduces the integrated fluxes from the three puncture scenarios.

4.3. Ruptures of buried pipelines

The base case full scale rupture modelled is a double ended guillotine break at the mid-point along a 96 kilometre length of below ground transportation pipeline, with external diameter of 0.61 m and pipeline wall thickness of 19.4 mm. The pipeline has a 1.2 m depth of clay soil cover. Valves are located 8 kilometres upstream and 8 kilometres downstream of this break. Valve closure begins after 900 s and the valve closure time is 30 s. At the time of the break, the pipeline is assumed to be filled with stationary dense phase CO_2 at an initial pressure at the upstream end of the pipeline of 150 barg and temperature of 30 ^oC. We employ predictions of the pipeline outflow calculated by University College London, UCL (Mahgerefteh, private communication) over the 2 hour release period in order to model behaviour in the crater. It is not possible to computationally simulate the entirety of this 2

hour period in detail as the resources required, in terms of number of processors and processing time, are too great, even for the highly efficient code used here. Therefore several snapshots during the decompression period are considered. In discussion with DNV GL (Cleaver, private communication), these snapshots were specified at t=30s, 100s, 250s, 600s, 1000s and 1150s for the base case scenario. These snapshots cover the smooth decompression prediction from UCL, and straight lines placed between these points approximate the decompression reasonably well. The snapshots at 1000s and 1150s were chosen in order to bracket the time at which the valve closure has an effect on the flow into the crater. At 1150s, the downstream pipe inflow rate drops below the triple point and the majority of the inventory has been released, hence no more snapshots were simulated after this time.

The geometry of the crater is assumed to be shaped like a 'bath tub' with length L and width W, with a horizontal rectangular section at its base of length L' and width W'. The length of the flat section is assumed to be equal to the fracture length and its width is assumed to be equal to the circumference of the pipeline, centred on the original position of the pipeline, as if a section of the pipeline has fractured open and then unrolled, leaving the neighbouring sections intact. As a first order modelling scenario, this represents the worst case failure of a pipeline reasonably well. Other failure scenarios will result in lower, less collimated, flows. The flat base is at the maximum crater depth, D. The ends of the flat base are flat ellipses. The method for joining the flat section of the crater to the crater rim in a smooth manner is based on ellipses calculated from the dimensions and wall angle of the crater, ensuring a smooth change of depth and the defined crater wall angle perpendicular to the pipeline at all positions along the rim. The dimensions of the crater have been estimated using the DNV-GL COOLTRANS (Cleaver, private communication) crater formation predictive model, based on real craters generated in full scale experiments and incidents.

Table 1. Integrated fluxes on a full horizontal plane above the crater for the punctures [15] and base case rupture.

	Case:	Puncture location:-			Base case rupture at time:-					
		Side	Base	Top	30s	100s	250s	600s	1000s	1150s
Mass-flow / kg s^{-1}	Total up	67.2	109.0	51.4	12668	9825	6991	5291	4331	4083
	Total down	26.6	0.78	0.0	1028	1710	1956	1189	1145	1360
	CO_2 up	40.1	49.5	50.3	7549	5809	4324	2986	2600	2373
	CO_2 down	0.45	0.25	0.0	15.76	43.80	48.92	134.5	200.0	145.3
	Solid up	9.68	8.58	16.5	1442	1014	801.2	454.8	443.3	501.6
	Solid down	0.003	0.016	0.0	0.02	0.064	0.006	0.197	1.54	0.404
Frac. / kg/kg	CO_2 up	0.597	0.454	0.979	0.596	0.591	0.618	0.564	0.600	0.581
	CO_2 down	0.017	0.32	-	0.015	0.026	0.025	0.071	0.136	0.107
	Solid up	0.241	0.173	0.328	0.191	0.175	0.185	0.152	0.171	0.211
	Solid down	0.007	0.064	-	0.001	0.001	0.0	0.001	0.008	0.002
Momentum / kg m s^{-2}	Total up	912.0	657.5	757.4	914000	637000	415000	233000	171000	155000
	Total down	136.8	0.23	0.0	4388	11900	18500	19500	9350	8740
	CO_2 up	560.5	294.2	751.6	600000	444000	290000	142000	107000	94400
	CO_2 down	1.62	0.074	0.0	82.4	238.8	243	1460	1210	972
	Solid up	141.5	53.3	249.2	126000	93200	62000	25600	20000	21200
	Solid down	0.001	0.005	0.0	0.111	0.307	0.004	2.190	8.018	2.386
Vel'y / m s^{-1}	Inferred up	13.57	5.77	14.74	72.1	64.9	59.3	44.1	39.5	37.9
	Inf. CO_2 up	13.98	5.94	14.94	79.5	76.4	67.1	47.7	41.3	39.8
	Inf. solid up	14.62	6.21	15.10	87.1	91.9	77.4	56.3	45.2	42.3
	Peak	22.48	9.4	27.8	188	129	164	150	141	134
Flow-weighted temp. / K		179.73	176.5	195.2	192.0	187.5	189.3	186.0	188.0	186.7

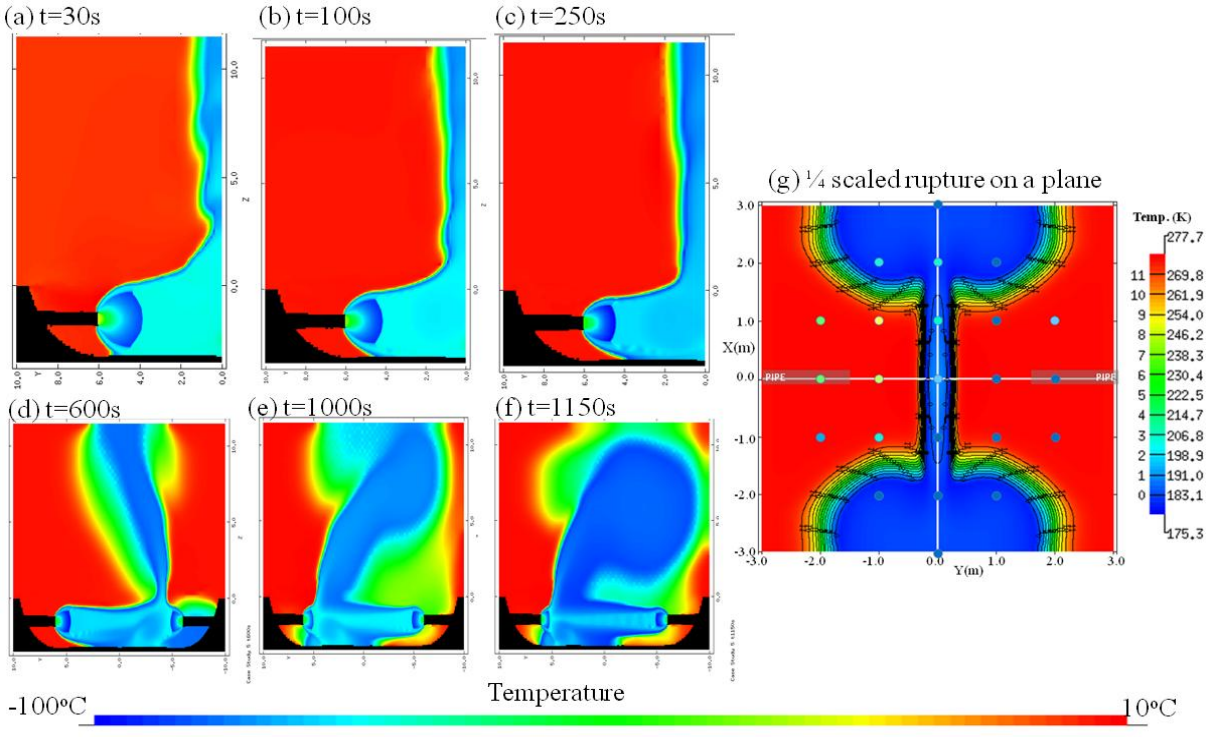

Figure 4. Snapshots of simulated temperatures on a vertical plane through the centre of the base case parallel to the pipeline. Snapshots are shown at times t = 30s (a), 100s (b) , 250s (c), 600s (d), 1000s (e) and 1150s (f). In Panel (g) a comparison between a simulation and the ¼ scaled rupture experiment is shown. Temperature is shown in the colour contour plot. Experimental data are indicated by round dots, colour –coded by temperature. Broad quantitative and qualitative agreement can be seen, although it would appear the experimental jets is pushed toward the pipe in the same manner as shown in panels (d) to (f).

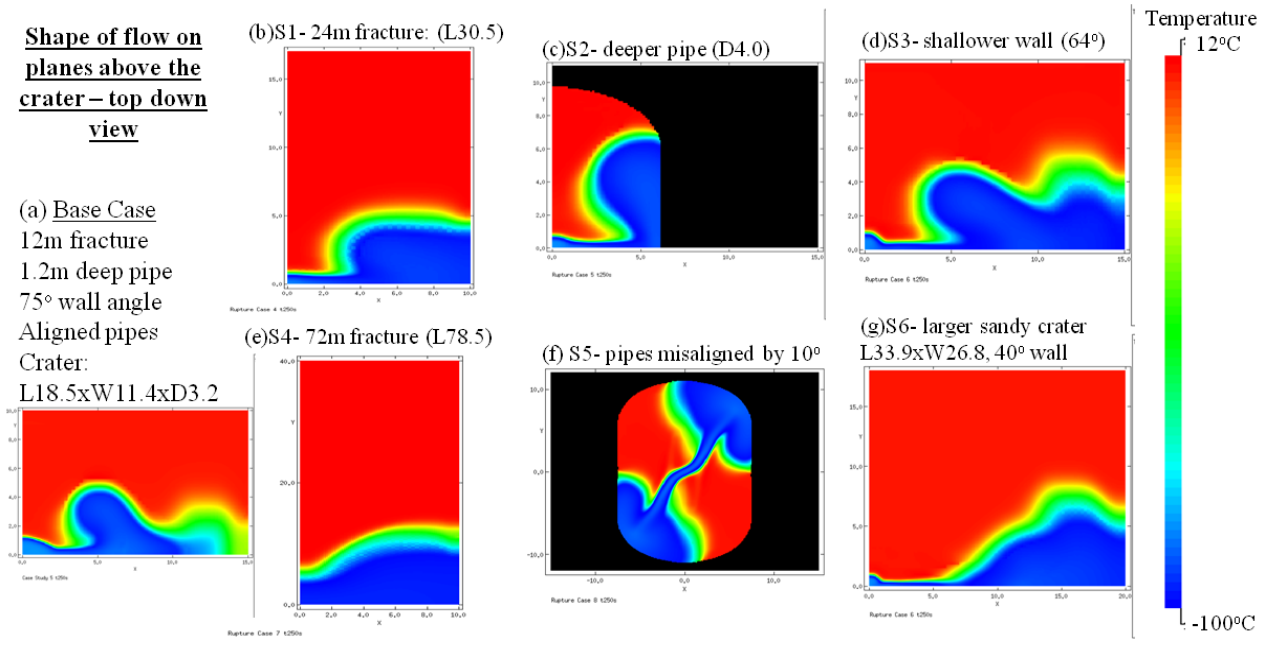

Figure 5. Snapshots of simulated temperatures on a horizontal plane above the crater at t=250 s into the base case rupture (a) and equivalent times in the sensitivity studies (b)-(f), varying crater parameters as detailed in each figure title.

In Figure 4, slices of the temperatures in the flow are shown at the different snapshot times. The predicted steady state flow through the crater on a vertical slice through the centre of the crater at the midpoint of the rupture, parallel to the initial velocity vector and on the x=0 m plane is shown in Figure 4(a). The expansion zone at the point of rupture as the fluid exits the pipeline is clear. In this region, the lowest temperatures are reached, passing below the triple point and freezing remaining liquid CO_2 into the solid phase. Just before the Mach shock at the termination of this zone, the highest velocities are reached, on the order of 400 ms^{-1}. Beyond the Mach shock, the temperature in the flow is at the sublimation temperature as the homogeneous equilibrium model enforces this if solid and gas phases are present in pure CO_2. Velocities have dropped to ~100 ms^{-1}. The temperature drops slowly as air is mixed into the jet, particularly as the plume exits the crater. The solid fraction just beyond the Mach shock is around 0.35 and this only begins to drop outside the crater. In the other panels, the same snapshot geometries are shown at later times. As the pressure at the pipe outlet drops with time, the size of the Mach shock and expansion zone clearly decreases, but the temperatures in the flow still remain very cold. Once the pipe flows become unbalanced (t=600 s and later), the jet flow out of the crater changes. Specifically it moves away from the centre of the crater toward one pipe end or the other. Initially it moves as might be expected towards the lower pressure downstream pipe end. Later, counter intuitively, it moves back towards the high pressure upstream pipe, which can be understood in terms of the downstream jet containing similar amounts of momentum to the upstream jet, but in a smaller cross-sectional area and therefore the downstream jet is able to force the crater outflow back towards the upstream pipe inlet. There is evidence for this in the scaled rupture experiments carried out by DNV GL, as shown in Figure 4(g), where also quantitative and qualitative agreement can be seen between the experiment and this prediction.

In Figure 5, we present results of the sensitivity survey, where crater parameters are varied in the manner detailed in the figure and also in Table 2. This sensitivity study on the base case has shown how different crater parameters affect the flow out of the crater. It is reasonable to conclude that the greatest effect comes from misaligning the pipes, although the S5 case considered is an extreme one and would require further studies to investigate the impact of, and corresponding changes to, the crater geometry caused by the release. Otherwise, a much increased fracture length (on the order of 72m in S4) has a large effect on the flow structure and on the integrated profiles, as shown in Table 2. Changing the pipe section length (S1), pipe depth (S2), crater wall angle (S3) or soil type (S6) have effects on the flow structure that can be understood in terms of the parameter change, but relatively minimal effects on the integrated fluxes shown in Table 2.

Table 2. Integrated flux comparisons for the base case and sensitivity studies.

#	Description	Plane height	CO_2 fraction	Solid fraction of CO_2 fraction	Average velocity	Peak velocity	Temperature
	Base case	2m	62%	18%	60 m s^{-1}	164 m s^{-1}	189 K
S1	24m fracture	2m	52%	13%	62 m s^{-1}	148 m s^{-1}	187 K
S2	Deeper pipe	0m	62%	18%	73 m s^{-1}		188 K
S3	64^o wall angle	2m	55%	15%	50 m s^{-1}		188 K
S4	72m fracture	6m	42%	6%	17 m s^{-1}	30 m s^{-1}	186 K
S5	Misaligned pipes	0m	63%	19%	43 m s^{-1}	140 m s^{-1}	188 K
S6	Sandy soil	1m	54%	15%	54 m s^{-1}		188 K

5. Conclusions

Application of a novel CFD model to predicting the near-field structure of high pressure releases of dense phase CO_2 has been presented, including validation against new experimental data representative of dense phase and gas phase CO_2 field-scale releases arising from deliberate venting, punctures and ruptures of CO_2 pipelines. The model developed has yielded good predictions of the characteristics of these jets, in comparisons with temperature data obtained from the experimental tests undertaken by DNV GL as part of the National Grid COOLTRANS research programme. It is clear from the results obtained that in order to accurately predict the near-field structure of such jets, a non-ideal equation of state which correctly accounts for the solid phase is required. Significant solids are

generated within the near-field of the jet, despite the pipeline release itself containing no solid phase CO_2 material. Hence integrated fluxes have been presented for this range of venting, puncture and rupture scenarios in order to provide the basis of robust source conditions for use in CFD studies of far-field dispersion and for use with pragmatic quantified risk assessment (QRA) models. This work demonstrates the capability of this full three-dimensional computational fluid dynamic tool to accurately predict multi-phase high pressure CO_2 discharges.

Acknowledgements

During the undertaking of this work as part of the COOLTRANS research programme, CJW was supported by National Grid, and CJW and MF would like to thank National Grid for their support of the work described herein. We acknowledge the provision of information regarding the experiments from DNV GL (D. Allason, K. Armstrong and R.P. Cleaver) and of pipe inlet conditions from UCL (V. Sundara, S. Brown and H. Mahgerefteh). National Grid initiated the COOLTRANS research programme as part of the Don Valley CCS Project in order to address knowledge gaps relating to the safe design and operation of onshore pipelines for transporting dense phase CO_2 from industrial emitters in the UK to storage sites offshore. The Don Valley CCS Project is co-financed by the European Union's European Energy Programme for Recovery (EEPR). The sole responsibility of this publication lies with the authors. The European Union is not responsible for any use that may be made of the information contained therein.

References

[1] Falle SAEG. AMR applied to non-linear elastodynamics. In: Plewa T, Linde T, Weirs VG, editors. Proceedings of the Chicago Workshop on Adaptive Mesh Refinements Methods, Springer Lecture Notes in Computational Science and Engineering. Springer, New York, USA. 41;235-253.

[2] Jones WP, Launder BE. The prediction of laminarization with a two-equation model of turbulence. International Journal of Heat and Mass Transfer 1972;15: 301-314.

[3] Fairweather M, Ranson KR. Prediction of underexpanded jets using compressibility-corrected, two-equation turbulence models. Progress in Computational Fluid Dynamics 2006;6:122-128.

[4] Sarkar S, Erlebacher G, Hussaini MY, Kreiss HO. The analysis and modelling of dilatational terms in compressible turbulence. Journal of Fluid Mechanics 1991;227: 473-493.

[5] Falle SAEG. Self-similar jets. Monthly Notices of the Royal Astronomical Society 1991;250:581-596.

[6] Harten A, Lax PD, van Leer B. On upstream differencing and Godunov-type schemes for hyperbolic conservation laws. SIAM Review 1983;25:35-61.

[7] Peng D-Y, Robinson DB. A new two-constant equation of state. Industrial and Engineering Chemistry Fundamentals 1976;15:59-64.

[8] Span R, Wagner W. A new equation of state for carbon dioxide covering the fluid region from the triple-point temperature to 1100 K at pressures up to 800 MPa. Journal of Physical and Chemical Reference Data 1996;25:1509-1596.

[9] Wareing C, Woolley RM, Fairweather M, Falle SAEG. A composite equation of state for modelling of sonic carbon dioxide jets in carbon capture and storage scenarios. American Institute of Chemical Engineers Journal 2013;59:3928-3942.

[10] Wareing C, Fairweather M, Peakall J, Keevil G, Falle SAEG, Woolley RM, Numerical modelling of particle-laden sonic CO_2 jets with experimental validation. In: Zeidan D, editor. AIP Conference Proceedings of the 11th International Conference of Numerical Analysis and Applied Mathematics. AIP Publishing 2013;1558:98-102.

[11] Allason D, Armstrong K, Cleaver P, Halford A, Barnett J. Experimental studies of the behaviour of pressurised release of carbon dioxide. In: Institute of Chemical Engineers Symposium Series No. 158, IChemE Publishing; 2012. p. 142-152.

[12] Cooper R. National Grid's COOLTRANS research programme. Journal of Pipeline Engineering 2012;11:155-172.

[13] Wareing CJ, Fairweather M, Falle SAEG, Woolley RM. Validation of a model of gas and dense phase CO_2 jet releases for carbon capture and storage application. International Journal of Greenhouse Gas Control 2014;27:254-271.

[14] Woolley RM, Fairweather M, Wareing CJ, Falle SAEG, Proust C, Hebrard J, Jamois D. Experimental measurement and Reynolds-averaged Navier-Stokes modelling of the near-field structure of multi-phase CO_2 jet releases. International Journal of Greenhouse Gas Control 2013;18:139-149.

[15] Wareing CJ, Fairweather M, Falle SAEG, Woolley RM. Modelling punctures of buried high-pressure dense phase CO_2 pipelines in CCS applications. International Journal of Greenhouse Gas Control, *accepted for publication*, 2014.